PROCEEDINGS OF SCIENCE

Nucleus and Hypernucleus Measurements with HADES

Heidi Schuldes[*a], **Timo Scheib**[a] **and Manuel Lorenz**[a] **for the HADES-Collaboration**
[a]*Goethe University Frankfurt*
E-mail: h.schuldes@gsi.de, t.scheib@gsi.de, m.lorenz@gsi.de

We present transverse momentum spectra of protons and deuterons measured with HADES in the reaction Ar(1.76 AGeV)+KCl demonstrating its light fragment reconstruction abilities. Furthermore we describe the analysis procedure for the reconstruction of the lightest hypernucleus, the hypertriton, using detailed GEANT simulations.

International Winter Meeting on Nuclear Physics,
21-25 January 2013
Bormio, Italy

[*]Speaker.

PoS(Bormio 2013)026

1. Introduction

The investigation of rare and penetrating probes in heavy-ion collisions (HIC) has attracted much interest in the recent years over all accessible collision energies. The ultimate hope is to find key observables sensitive to the onset of deconfinement, the critical point and chiral symmetry restoration. In the energy regime of a few GeV, strange hadrons are particularly suitable probes of the high density phase of nuclear matter. Due to the conservation of the strangeness quantum number, its production is a highly associated process. An exact description of all multiplicities of particles with strangeness content and their excited states is necessary to fully understand their in-medium production and propagation. The HADES collaboration has published an unmatched number of hadron yields from the Ar+KCl data for this energy regime [2, 3, 4, 5]. The analysis of the hypertriton will extend the study of strange particles to hypernuclei production. The spectroscopy of hypernuclei, i.e. nuclei containing at least one hyperon, provides an ideal tool to study the YN interaction, which is partly responsible for the binding of hypernuclei and hence their life-time. Recently, also data from relativistic heavy ion collisions have been published, most prominently the discovery of the anti-hypertriton by the STAR collaboration at a center of mass energy of $\sqrt{s_{NN}}$ =200 GeV [8]. But also at lower energies, like those in the SIS18 regime, with available beam energies of 1-2 AGeV, experimental programs, e.g. HypHi [7], are developed. Such studies are of great interest as they are not limited to hypernuclei close to the valley of β stability.

The interpretation of HIC by means of theoretical models needs to be contrasted to global event characteristics, probing the dynamics of the collision. Rapidity distributions of protons and heavier fragments, such as d and t, comprise a direct view on the HIC dynamics. At SIS energies valuable systematics have been collected and published by the FOPI collaboration in [9] mostly for central Au+Au collisions. Data of HADES on Ar+KCl at 1.76 AGeV extends this study to a system of medium size. As one of the most probable production mechanisms of the hypertriton is nucleon coalescence of a Λ baryon and a light fragment, like for example $\Lambda + d \rightarrow {}^{3}_{\Lambda}H$ [10], its study connects strangeness production directly to global event properties, like for example the rapidity distribution of light fragments.

2. Experimental Setup

The High-Acceptance Di-Electron Spectrometer (HADES) is a charged-particle detector consisting of a 6-coil toroidal magnet centered on the beam axis and six identical detection sections located between the coils and covering polar angles between 18° and 85°. Each sector is equipped with a Ring-Imaging Cherenkov (RICH) detector followed by Multi-wire Drift Chambers (MDCs), two in front of and two behind the magnetic field, as well as a scintillator hodoscope (TOF/TOFino). Hadron identification is based on the time-of-flight and on the energy-loss information from TOF/TOFino, as well as from the MDC tracking chambers. A detailed description of HADES is given in [11].

For the presented data an argon beam of $\sim 10^6$ particles/s was incident with a beam energy of 1.76 AGeV on a four-fold segmented KCl target with a total thickness corresponding to 3.3 % interaction probability. A fast diamond start detector located upstream of the target was intercepting the beam and was used to determine the time-zero information. The data readout was started by a first-

level trigger (LVL1) requiring a charged-particle multiplicity, $MULT \geq 16$, in the TOF/TOFino detectors. Based on a full GEANT simulation of the detector response to Ar+KCl events generated with the UrQMD transport model [12], we found that the event ensemble selected by this (LVL1) trigger condition has a mean number of participating nucleons ($\langle A_{part} \rangle$) equal to 38.5 ± 3.9.

3. Light Fragments

3.1 Particle Identification and Analysis

The particle identification is done using velocity vs. momentum $\times$ polarity correlations (see Fig. 1), where the velocity is determined by the time-of-flight measurement in the TOF and TOFino scintillators with respect to the time-zero information and the tracked flight path. If needed, additional particle discrimination is gained from the energy-loss (dE/dx) information in the MDC and scintillators. This is illustrated in Fig. 2 where the mass distribution in the TOF region is plotted after application of track quality selections (green) and after an additional selection on deuterons making use of the energy-loss information (blue).

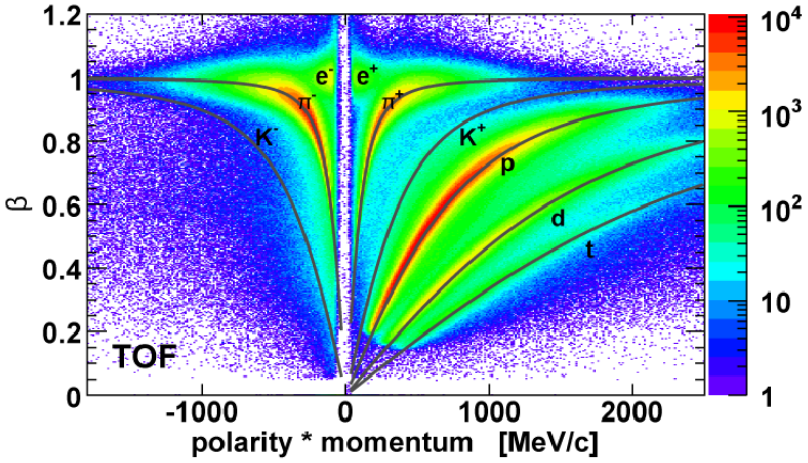

Figure 1: Velocity vs. momentum $\times$ polarity correlations in the TOF region.

The yields of the different particles are counted as a function of rapidity y and transverse momentum p_t. Efficiency and acceptance losses are corrected for a given y and p_t region iteratively using simulated data embedded into real events. In a first step the momentum distribution of the simulated particles was assumed to be a white distribution, while finally a distribution assuming a thermal source, which is very similar to the experimentally observed, was used. We find only little sensitivity to these inital conditions (at the order of 1% in the overall correction per given region). The combined correction factors for losses due to efficiency and acceptance as a function of p_t for a typical y region are displayed in Fig. 3 separately for p and d.
For further details about the particle identification and the data analysis of charged hadrons we refer to [13, 14, 15, 5].

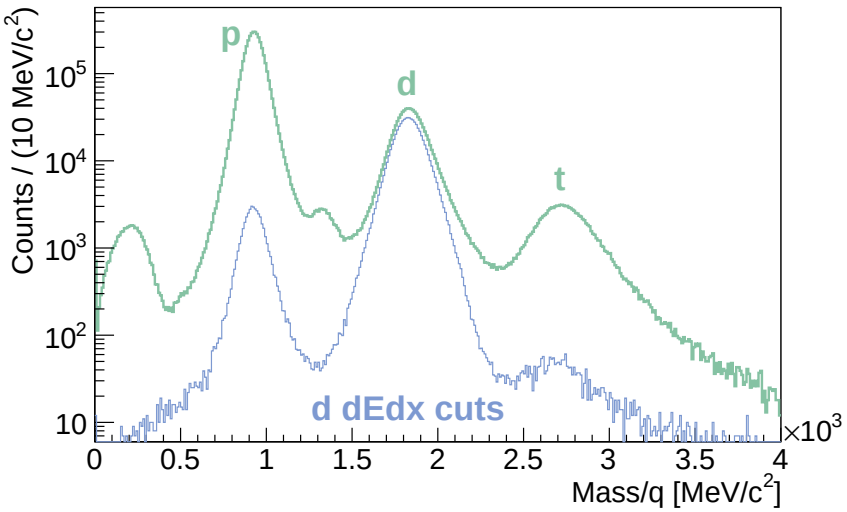

Figure 2: Mass distribution in the TOF region after application of track quality selections (green) and additional selection on deuterons making use of the energy-loss information (blue).

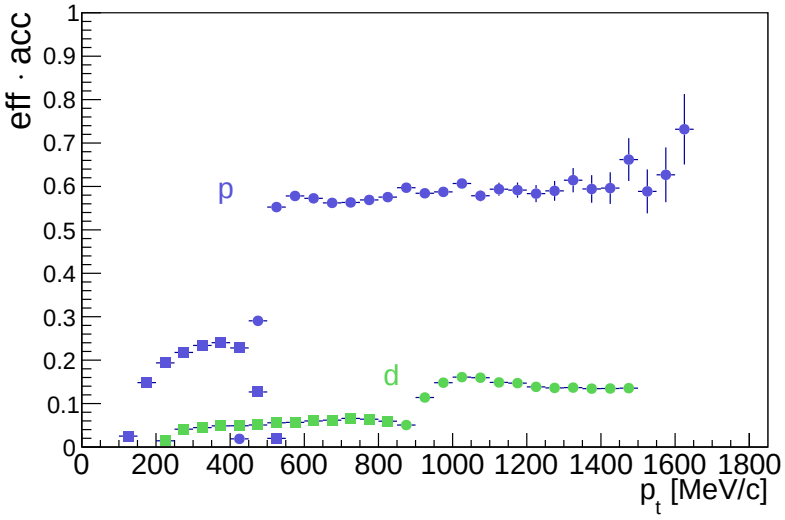

Figure 3: Combined correction factor for losses due to efficiency and acceptance in the TOF (circles) and TOFino region (squares) as a function of p_t for p (blue) and d (green) in the rapidity region $0.4 < y < 0.45$.

3.2 Phase-space Distributions

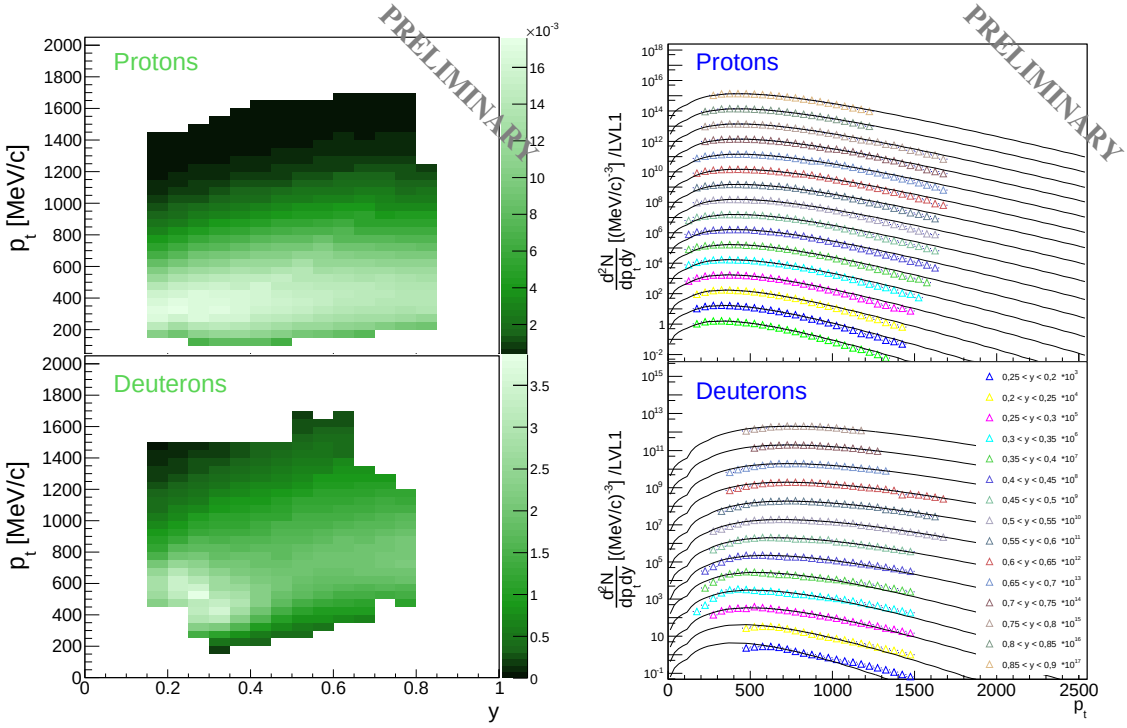

Figure 4: Efficiency and acceptance corrected phase-space distributions (left) and transverse momentum spectra for all measured rapidity regions (right) of protons (top) and deuterons (bottom). The transverse momentum spectra are scaled to get a clearer display. To extrapolate to the unmeasured transverse momentum regions, the spectra are fitted by the parametrization 3.1.

The resulting phase-space distributions as a function of transverse momentum and rapidity, and the transverse momentum spectra of p and d, as they are the most abundant particles, are displayed in Fig. 4. In order to extrapolate into the unmeasured regions the spectra are adapted using the model-independent function:

$$\frac{dN}{dp_t} = c \cdot p_t^n \cdot \exp(p_t/b), \tag{3.1}$$

whereas $n = 3$ for protons and $n = 4$ for deuterons.

This analysis shows that HADES is capable of identifying protons and light fragments like deuterons with excellent resolution. By combining the light fragment ^{3}He with a negatively charged pion the reconstruction of the lightest hypernucleus, the hypertriton, becomes possible. The analysis procedure will be summarized in the following section.

4. Hypertriton

4.1 Analysis

Hypertritons are most easily reconstructed through their decay into a negative pion and a ^{3}He. The branching ratio for this decay is about 35% [16]. Hence, an important issue of the analysis is a

good identification of the two final-state particles π^- and ^{3}He via the time-of-flight information in the TOF and TOFino walls and the energy loss in the Multiwire Drift Chambers as well as in the TOF and TOFino walls. The selection of ^{3}He is shown in Fig. 5. Cuts are applied on the quality of the tracks (χ^2_{RK}) and the energy-loss. In addition, double hits have been rejected in the inner time-of-flight wall TOFino since the double hit probability in this sub-detector was relatively high compared to previously investigated collision systems with HADES.

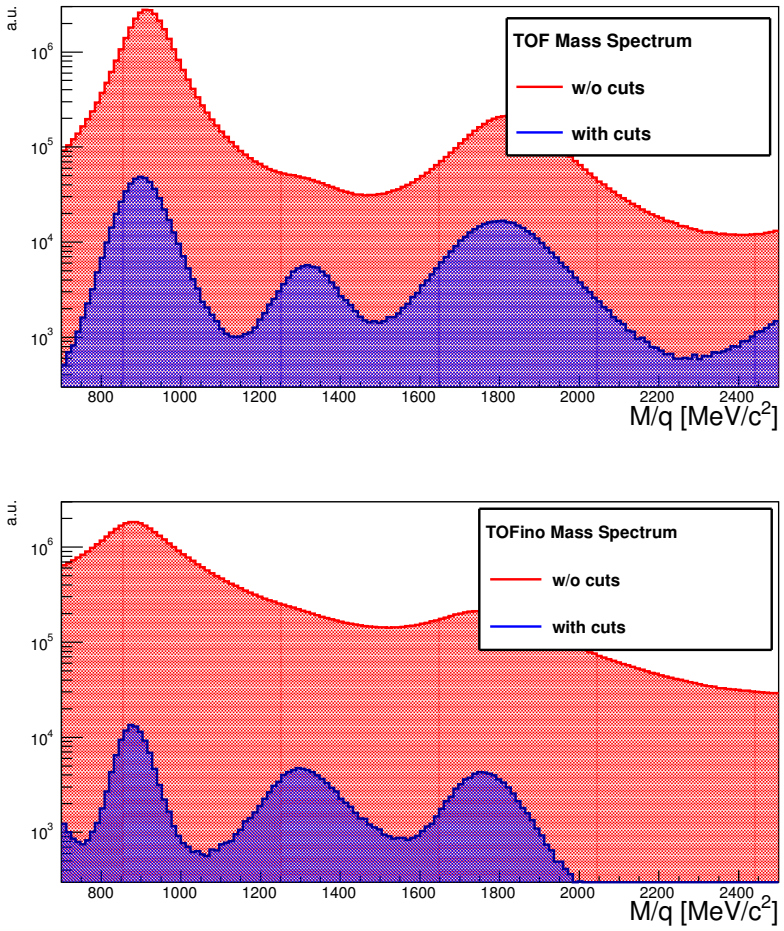

Figure 5: Mass distribution in the TOF- (top) and TOFino-region (bottom) before (red) and after application of cuts on the energy-loss of ^{3}He and additional track quality selections (blue).

In order to reduce the background stemming from uncorrelated pairs of negative pions and helium nuclei, secondary-vertex cuts are applied. The procedure is comparable to the $\Lambda \rightarrow \pi^- + p$ analysis in Ar+KCl [5].

For the background suppression constraints on the distance between the primary and the decay vertex (d_{V0}), on the distance between the π^- trajectory and the primary vertex (d_{π^-}), on the maximum distance between the two tracks of the decay particles (d_{dca}) and on the distance of the hypertriton particle track to the primary vertex ($d_{^3_\Lambda H}$) were made. Additionally, a lower limit was set to the opening angle ($\alpha_{\pi^- {}^3He}$) to improve the decay vertex resolution. The values of the selection

criteria are summarized in Tab. 1. For the optimization of the applied cuts, detailed Monte-Carlo simulation of the hypertriton decay including the detector response are used in order to observe their effects on the significance of the signal. The hypertritons are produced either thermally or via coalescence processes with Pluto [10]. For the coalescence production mechanism a rapidity distribution peaking close to target respectively beam rapidity is assumed, which is observed for the light fragments in this collision system. The detector response on the analyzed decay channel is simulated with HGeant, and to get a realistic estimate of the uncorrelated background, the simulated signal is again embedded into real events.

Topology quantity	d_{V0}	d_{π^-}	d_{dca}	$d_{^3_\Lambda H}$	$\alpha_{\pi^- {}^3He}$
Value	> 20mm	> 10mm	< 8mm	< 6mm	$> 17^\circ$

Table 1: Values of the cuts on the hypertriton decay topology.

Additionally, the acceptance and the reconstruction efficiency of the hypertriton are determined via simulations to $\text{acc} \cdot \text{eff}_{rec} = (0.041) \pm 0.002)\%$ for those produced via coalescence and $\text{acc} \cdot \text{eff}_{rec} = (0.060 \pm 0.006)\%$ for those coming from thermal sources.

The background of uncorrelated π^--^{3}He pairs is obtained by using the mixed-event method. Figure 6 shows the simulated invariant mass spectrum of ^{3}He and π^- with underlying mixed-event background. After subtracting the mixed-event background from the spectrum of the same event, a clear signal can be obtained, demonstrating the feasibility of the hypertriton reconstruction with HADES in the investigated channel.

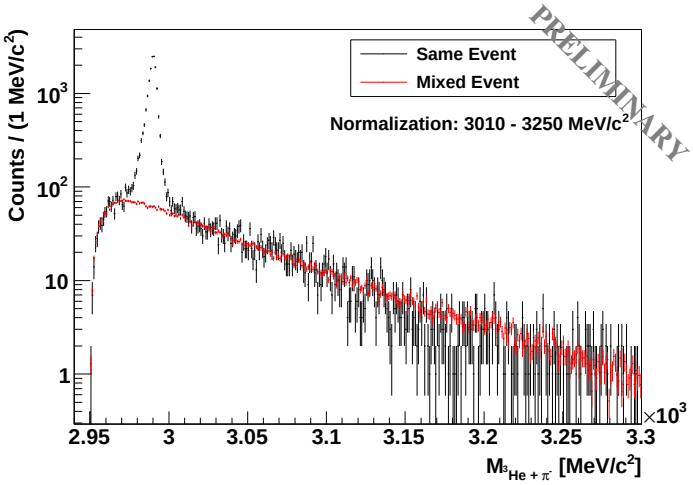

Figure 6: Invariant mass spectrum of ^{3}He and π^- candidates of simulated hypertriton decays embedded to real data with underlying mixed-event background.

4.2 Results

In Fig. 7, the invariant mass spectrum of π^-- and ^{3}He-candidates from the experimental data as well as the introduced mixed-event background are shown. After subtracting this background from real data there is no significant hypertriton signal visible.

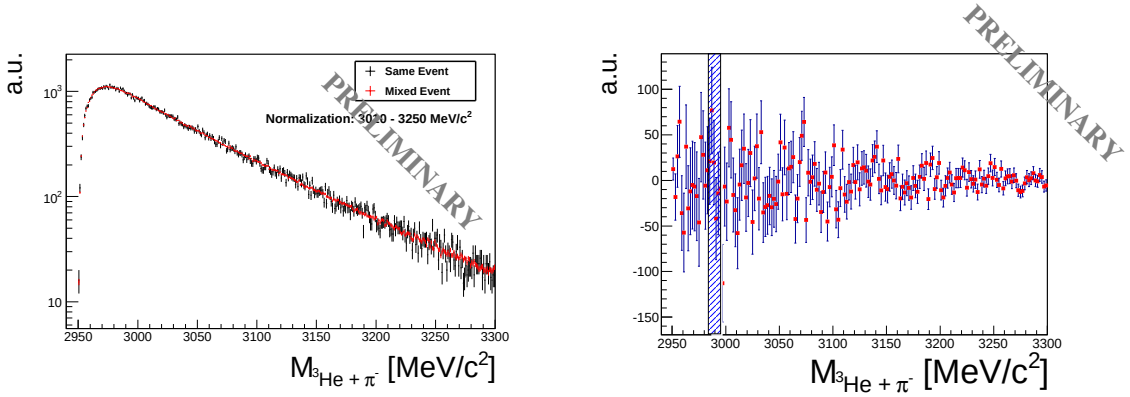

Figure 7: Left: Invariant mass spectrum of ^{3}He and π^- candidates from experimental data with underlying mixed-event background. Right: Invariant mass spectrum of ^{3}He and π^- candidates in real data after subtracting the background.

However, in principle an upper production limit can be calculated from the presented data sample using statistical methods like the one from Feldman-Cousins [19]. The results are currently completed will be presented shortly in an upcoming publication.

5. Summary

In summary we demonstrated the capabilities of HADES for reconstruction of p, d and hypertritons using simulations and data from Ar+KCl collisions at 1.76 AGeV. From the real data no significant hypertriton signal could be reconstructed. However an upper limit can be extracted and will be published soon.

Acknowledgements

We like to thank Y. Leifels, N. Herrmann and Y. Zhang for fruitful discussions. Work supported by BMBF 06FY9100I, 06FY7114, HIC for FAIR, HQM, HGS-Hire, EMMI and GSI.

References

[1] G. Agakishiev *et al.* (HADES Collaboration), Phys. Rev. C **84**, 014902 (2011).

[2] G. Agakishiev *et al.* (HADES Collaboration), Phys. Rev. C **80**, 025209 (2009).

[3] G. Agakishiev *et al.* (HADES Collaboration), Phys. Rev. C **82**, 044907 (2010).

[4] G. Agakishiev *et al.* (HADES Collaboration), Phys. Rev. Lett. **103**, 132301 (2009).

[5] G. Agakishiev *et al.* (HADES Collaboration), Eur. Phys. J. A **47** 21 (2011).

[6] T. R. Saito, D. Nakajima, C. Rappold, S. Bianchin, O. Borodina, V. Bozkurt, B. Gokuzum and M. Kavatsyuk *et al.*, Nucl. Phys. A **881** 218 (2012).

[7] C. Rappold, E. Kim, D. Nakajima, T. R. Saito, O. Bertini, S. Bianchin, V. Bozkurt and M. Kavatsyuk et al., carbon target at 2 AGeV," arXiv:1305.4871 [nucl-ex].

[8] B. I. Abelev [STAR Collaboration], Science **328** (2010) 58 [arXiv:1003.2030 [nucl-ex]].

[9] W. Reisdorf *et al.* (FOPI Collaboration), Nucl. Phys. A 848:366-427, (2010).

[10] J. Steinheimer, K. Gudima, A. Botvina, I. Mishustin, M. Bleicher *et al.*, Phys. Lett. B 714:85-91 (2012).

[11] G. Agakishiev *et al.* (HADES Collaboration), Eur. Phys. J. A **41**, 243 (2009).

[12] S. A. Bass *et al.*, Prog. Part. Nucl. Phys. **41** 225 (1998).

[13] A. Schmah, PhD thesis, Technical University Darmstadt, Darmstadt (2008).

[14] M. Lorenz, PhD thesis, Goethe-Universität, Frankfurt (2012).

[15] H. Schuldes, Master thesis, Goethe-Universität, Frankfurt (2012).

[16] H. Kamada, J. Golak, K. Miyagawa, H. Witala, W. Gloeckle, arXiv:nucl-th/9709035v1.

[17] I. Frohlich, T. Galatyuk, R. Holzmann, J. Markert, B. Ramstein, P. Salabura and J. Stroth, J. Phys. Conf. Ser. **219** (2010) 032039.

[18] GEANT. Detector Description and Simulation Tool, 2004. http://cont.cern.ch/writeup/geant/, Online User Guide.

[19] G. J. Feldman and R.D. Cousins, Phys. Rev. D57, 3873, 1998.